Back Analysis of the Draining Process of the Tangjiashan Barrier Lake

Zuyu Chen, Ph.D.[1]; Liqiu Ma, Ph.D.[2]; Shu Yu, Ph.D.[3]; Shujing Chen[4]; Xingbo Zhou[5]; Ping Sun, Ph.D.[6]; and Xu Li, Ph.D.[7]

Abstract: This study attempts to use a dam breach model to reproduce the well-monitored outflow hydrograph obtained during the dam breaching process of the Tangjiashan barrier lake, which was formed by a landslide triggered by the Wenchuan earthquake on May 12, 2008 in China. The key parameters that affect the model results, such as soil erosion and breach lateral enlargement, are reviewed by using field measurements followed by extensive sensitivity studies. The present paper advocates a hyperbolic model for soil erosion rate and a circular slip surface approach for breach lateral enlargement, which contribute to more reliable model results. The governing equations are solved using a numerical method that allows straightforward calculations coded in an Excel 2007 spreadsheet. This provides an easy, transparent, and robust tool that could enable practicing engineers to perform dam breach analyses with a comprehensive understanding of the uncertainties involved. This back analysis confirms that the peak outflow can be predicted with reasonable accuracy if the input values of the key model parameters are within well-understood ranges. **DOI: 10.1061/(ASCE)HY.1943-7900.0000965.**

Author keywords: Dam breach; Back analysis; Soil erosion rate; Barrier lake.

Introduction

The breaking of natural or synthetic dams often causes significant disasters, and the related research is in high demand. Estimation of the dam-break flood is of prime importance in such research, especially when dam safety emergency responses are concerned. Early examples of analytical models for peak breach outflow can be attributed to Cristofano (1965), followed by the works by Harris and Wagner (1967), Brown and Rogers (1977, 1981), Ponce and Tsivoglou (1981), MacDonald and Langridge-Monopolis (1984), Costa (1985), Fread (1988), Froehlich (1995), Walder and O'Connor (1997), Singh and Scarlatos (1988), Wang and Bowles (2006), Macchione (2008), Chang and Zhang (2010), and Wu (2013), among many others. State-of-the-art reviews on dam breach (Morris and Hassan 2002; Zhu et al. 2004; ASCE Task Committee 2011; Wahl 2010; Wu and Wang 2010) generally agree that the ability to predict the breach outflow is still far from advanced, demonstrating the following limitations and deficiencies:

1. Modeling the breaching process involves a large number of uncertainties: for example, failure modes (overtopping or piping), material properties (capabilities against erosion and collapse), and dam configurations (shapes, dimensions and structures) (Wurbs 1987; Zhu et al. 2004). It is important to conduct uncertainty analyses (Wahl 2004) using simulation models, such as the hydrologic engineering centers river analysis system (HEC-RAS) (HEC 2006a, b), which allow users to evaluate quickly the impacts of a variety of parameters on the results (Gee 2009).
2. Available data documenting historical dam-breach cases are limited and coarse, relying mostly on eyewitness reports in a few cases, e.g., the Teton dam in the United States (Zhu et al. 2004). Peng and Zhang (2012) highlighted this point based on information in a database of 1,239 landslide dams. Efforts have been made to perform large-scale prototype dam failure tests, such as the 6-m-high model dam used in the IMPACT project in Europe (Hassan and Morris 2008), and the 9.7-m-high model dam in China (Zhang et al. 2009). The scales of these models still cannot represent the real size of most existing prototype dams.
3. Considering that the rapid breaching process requires swift predictions for timely warning and decision making, the next generation of breach models should adopt simple, easy to use, and physically based methods (ASCE Task Committee 2011).

On May 12, 2008, a 90–124-m-high landslide dam with a barrier lake, which had a storage capacity of up to 32 million m^3, was created near Tangjiashan as a consequence of the magnitude 8.0

[1]Professor of Engineering, State Key Laboratory of Simulation and Regulation of Water Cycle in River Basin, Beijing 100048, China; and Dept. of Geotechnical Engineering, China Institute of Water Resources and Hydropower Research, Beijing 100048, China (corresponding author). E-mail: chenzuyu@cashq.ac.cn

[2]Postdoctoral Research Fellow, Guizhou Power Engineering Construction Supervision Company, Guiyang 550005, China; and Dept. of Geotechnical Engineering, China Institute of Water Resources and Hydropower Research, Beijing 100048, China. E-mail: lqmo_912@163.com

[3]Senior Engineer, State Key Laboratory of Simulation and Regulation of Water Cycle in River Basin, Beijing 100048, China; and Dept. of Geotechnical Engineering, China Institute of Water Resources and Hydropower Research, Beijing 100048, China. E-mail: yushu@iwhr.com

[4]Postgraduate Student, College of Architecture and Civil Engineering, Beijing Univ. of Technology, Beijing 100022, China. E-mail: 1023751816@qq.com

[5]Ph.D. Candidate, College of Water Resources and Hydropower Engineering, Xi'an Univ. of Technology, Xi'an 710048, China. E-mail: zhou_xingbo@126.com

[6]Senior Engineer, State Key Laboratory of Simulation and Regulation of Water Cycle in River Basin, Beijing 100048, China; and Dept. of Geotechnical Engineering, China Institute of Water Resources and Hydropower Research, Beijing 100048, China. E-mail: sunping@iwhr.com

[7]Associate Professor, School of Civil Engineer, Beijing Jiaotong Univ., Beijing 100044, China. E-mail: ceXuLi2012@gmail.com

Note. This manuscript was submitted on November 13, 2013; approved on October 2, 2014; published online on December 10, 2014. Discussion period open until May 10, 2015; separate discussions must be submitted for individual papers. This paper is part of the ***Journal of Hydraulic Engineering***, © ASCE, ISSN 0733-9429/05014011(14)/$25.00.

Wenchuan earthquake in the southwest Sichuan Province of China (Liu et al. 2009, 2010). More than 1,000 soldiers and technical staff, conveyed by helicopters, worked desperately in an inaccessible area to excavate a channel lowering the dam crest by 13 m and initiated a carefully monitored artificial draining process. Initial predictions using various empirical parametric models generally overestimated the peak outflow. For example, one prediction as described by Liu et al. (2009) employed a weir flow formula and predicted a peak discharge of 46,000 m^3/s, which was eight times that of the actual measured magnitude. The inability to provide reliable dam-breach flood estimation resulted in a decision to evacuate 275,000 people (Liu et al. 2010). A case report documenting these data has been published previously in this journal (Liu et al. 2010). The present paper is a continuation of that earlier work, aiming to reproduce the measured breach flow hydrograph based on the parameters interpreted from field measurements and the dam-breach models that have been well established by many researchers (e.g., Fread 1984; Singh 1996; Wu 2013). In the used breach model, a simple numerical algorithm, which essentially avoids the need for iterations at each time increment, has been developed using an Excel 2007 spreadsheet. Sensitivity studies have been performed extensively and offered improved understanding of the uncertainties involved in dam-breach analysis.

Review of Draining Process and Monitored Data

The landslide debris dam was approximately 90 m high on the right-hand side, with a water storage capacity of 230 million m^3 and a water level of 742.5 m above sea level when the dam breaching started on June 10, 2008.

The first author of this paper, who is the corresponding author of Liu et al. (2010), is able to reorganize the original data collected in the field. Table 1 presents the monitored data that include (1) reservoir water level, H, obtained by an automatic hydro-gauge station connected to China's Beidou (COMPASS) Navigation Satellite System (Column 7); (2) average flow velocity, V, near the entrance of the channel, which is based on surface velocity measurements using a Decatur radar laser hydrometer (Column 4); (3) water surface width, B, obtained using a Nikon Laser 800S Range Finder (Column 5); and (4) cross-sectional area, A, (Column 3), which was calculated based on the flow depths measured by multipoint S48-1 ultrasonic wave depth measurement instruments over the cross section. The average flow depth h is equal to A divided by B, which is presented in Column 6. It should be noted that the measurement of reservoir water level H, which was performed independently in a gauge station, was not contemporaneous to the measurements of the other hydraulic parameters. The data of H listed in Column 7 are based on interpolations.

Although significant effort was made to collect the data, the information was still found incomplete for the present study. It is noted that no measurement was performed on the water-surface drop at the entrance to the channel, which is a parameter in dam-breach analysis regarding the influence of head loss at the entrance. To compensate for this omission, an additional calculation has been performed. By neglecting the approaching velocity and water head loss in front of the entrance, the energy balance equation can be expressed as

Table 1. Field Measurement and Interpretations of the Hydraulic Parameters

	Field measurements								Interpretations						
Number	1	2	3	4	5	6	7	8	9	10	11	12	13	14	15
Date	Time	Q (m^3/s)	A (m^2)	V (m/s)	B (m)	h (m)	H (m)	H-H' (m)	H' (m)	$z = H' - h$ (m)	H-z (m)	$m = h/(H$-$z)$	Q/B (m^3/s-m)	τ (Pa)	dz/dt (mm/s)
8 June	7:28	5.72	11	0.52	7.0	1.57									
	10:00	8.26	10.2	0.81	7.0	1.46									
	12:08	18.1	8.5	2.13	7.0	1.21									
	15:00	24.8	12.4	2.01	9.0	1.38									
	19:00	28.9	12.5	2.32	9.5	1.32									
9 June	7:36	55.9	19.6	2.85	11.5	1.70	742.55	0.41	742.14	740.43	2.12	0.80	4.86	41.65	
	12:30	76.1	28	2.72	12.5	2.24	742.70	0.38	742.32	740.08	2.62	0.86	6.09	34.63	
	17:30	93.3	33.9	2.75	14.0	2.42	742.80	0.39	742.41	739.99	2.81	0.86	6.66	34.49	
10 June	1:30						743.10			740					
	6:00	574	243	2.36	35.0	6.94	742.46	0.28	742.18	735.2	7.23	0.96	16.40	17.88	
	8:16	843	337	2.5	45.0	7.49	742.18	0.32	741.86	734.4	7.81	0.96	18.73	19.57	0.11
	8:36	1090	383	2.85	51.0	7.51	742.18	0.41	741.76	734.3	7.92	0.95	21.37	25.41	0.10
	9:06	1400	478	2.93	59.0	8.10	742.17	0.44	741.74	733.6	8.54	0.95	23.73	26.18	0.34
	9:30	2030	508	3.99	63.0	8.06	742.17	0.81	741.36	733.3	8.87	0.91	32.22	48.63	0.23
	10:00	2530	549	4.61	67.0	8.19	740.51	1.08	739.43	731.2	9.28	0.88	37.76	64.57	1.15
	10:30	5110	866	5.9	73.0	11.86	739.04	1.77	737.26	725.4	13.64	0.87	70.00	93.49	(3.24)
	11:00	5980	1223	4.89	129	9.48	737.56	1.22	736.34	726.9	10.70	0.89	46.36	69.20	(−0.81)
	11:12	6000	1222	4.91	129	9.47	736.85	1.23	735.62	726.2	10.70	0.89	46.51	69.79	0.99
	12:00	6070	1275	4.76	130	9.81	734.02	1.15	732.87	723.1	10.96	0.89	46.69	64.83	1.07
	12:30	6500	1310	4.96	130	10.08	732.25	1.25	731.00	720.9	11.33	0.89	50.00	69.76	1.19
	13:00	6130	1310	4.68	132	9.92	730.48	1.12	729.36	719.4	11.04	0.90	46.44	62.43	0.82
	14:00	4480	1117	4.01	145	7.70	727.94	0.82	727.12	719.4	8.52	0.90	30.90	49.87	0.01
	15:00	3040	688	4.42	145	4.74	725.80	1.00	724.80	720.1	5.74	0.83	20.97	71.21	(−0.18)
	16:00	1940	515	3.77	145	3.55	723.75	0.72	723.03	719.5	4.28	0.83	13.38	57.06	0.16
	17:00	1040	312	3.33	145	2.15	722.58	0.57	722.01	719.9	2.72	0.79	7.17	52.61	(−0.11)
	18:00	653	239	2.73	145	1.65	721.40	0.38	721.02	719.4	2.03	0.81	4.50	38.64	0.14
	19:00	524	206	2.54	145	1.42	720.25	0.33	719.92	718.5	1.75	0.81	3.61	35.15	0.24
	20:00	335	138	2.42	80.0	1.73	719.48	0.30	719.18	717.5	2.02	0.85	4.19	29.91	0.29

Note: A = area; B = width; dz/dt = erosion rate; H = reservoir water level; H' = channel water level; $H - H'$ = hydraulic drop; h = depth of water in channel; m = correction ratio for head loss; Q = discharge; Q/B = discharge per unit width; V = average velocity; z = chanel bed level; τ = shear stress.

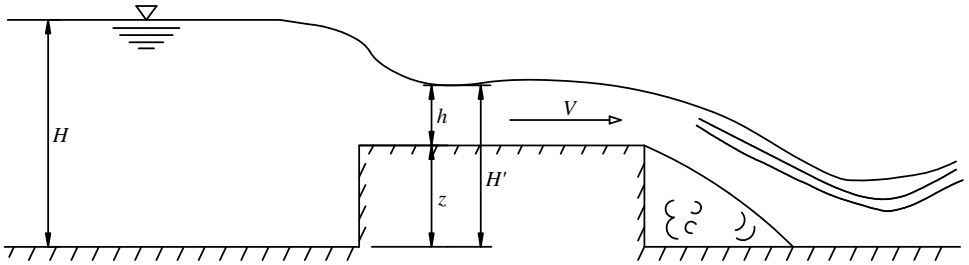

Fig. 1. Hydraulic relations at entrance of channel

$$H = z + h + \frac{V^2}{2g} = H' + \frac{V^2}{2g} \tag{1}$$

where H' and z = elevations of the channel water surface and bottom, respectively (Fig. 1); and g = gravitational acceleration. As V had already been measured, the elevation of the channel water surface H' (Column 9 in Table 1) can be calculated by substituting the values of measured V and H into Eq. (1).

The missing information regarding the hydraulic drop $(H - H')$ can then be estimated by

$$H - H' = \frac{V^2}{2g} \tag{2}$$

The relevant information is shown in Column 8 of Table 1. Furthermore, z (Column 10) can be calculated by $(H' - h)$, where h (Column 6) is known.

The soil erosion rates $\Delta z/\Delta t$ and the associated shear stresses applied on the channel bed are of prime interest in establishing the dam-breach analysis methods. The shear stresses, as shown in Column 14, are calculated using the following widely used equation (e.g., Macchione 2008; Gaucher et al. 2010)

$$\tau = \gamma R' J = \frac{\gamma n^2 V^2}{R'^{1/3}} \approx \frac{\gamma n^2 V^2}{h^{1/3}} \tag{3}$$

where γ = density of water; n = roughness coefficient (0.025 $m^{-1/3}$ in this case); J = slope of the channel; and R' = hydraulic radius that can be approximated by h if the channel width B is sufficiently larger than the average flow depth h (Guo and Jin 1999). Column 15 presents the erosion rates $\Delta z/\Delta t$ measured in the field, among which the bracketed data are believed questionable and excluded in the following studies.

Table 1 reveals that following June 8, the depth and width of the flow in the channel started to increase gradually. However, the reservoir water level H kept rising because of the natural inflow of about 80 m^3/s. It reached a maximum value of 743.1 m at 1:30 a.m. on June 10. Then records were missing until 8:00 a.m. on June 10 when H was 742.18 m. It then dropped rapidly between 9:00 and 9:30 a.m. from 742.17 to 740.50 m. From 1:30 a.m. to 9:30 a.m., the measured velocity V was between 2.3 and 2.9 m/s. The corresponding shear stress was between 20 and 30 Pa (N/m^2). It may be presumed that dam breach started sometime between 1:30 a.m. and 8:00 a.m. on June 10, and the incipient velocity was around 2.6 m/s associated with a flow depth h of 6–7 m. The average shear stress was presumed around 20–30 Pa. The peak outflow measured was 6,500 m^3/s at 12:30 p.m. The average erosion rate of the channel bed from 1:30 a.m. to 12:30 p.m., when the peak discharge developed, was 1.8 m/h or 0.50 mm/s, which is associated with a flow velocity of between 2.4 and 5.9 m/s and shear stresses of 20–80 Pa. The peak erosion rate was 1.19 mm/s.

Dam-Breach Analysis Model

A brief description of the key aspects involved in the adopted breach analysis model in conjunction with evaluation and discussions of parameters based on the evidence from Tangjiashan is given here.

Broad-Crested Weir Flow Analysis

Like in most of dam breach models, the outflow through the breach is estimated using the hydraulics of a broad-crested weir. In general, it is expressed by the following equation for a channel with a rectangular cross section

$$Q = CB(H - z)^{3/2} \tag{4}$$

where C = discharge coefficient whose theoretical value is 1.7 $m^{1/2}/s$ (Singh 1996). Previous researchers have adopted values of C ranging from 1.3 to 1.7 (Jack 1996). When the breach process approaches its end and the reservoir water level is close to that of the downstream tailwater, a coefficient that accounts for the effect of submergence is introduced (Fread 1988; Singh et al. 1988). A number of researchers adopt a lumped coefficient for C in Eq. (4) in their calculations (Harris and Wagner 1967; MacDonald and Langridge-Monopolis 1984; Chang and Zhang 2010). This value can be determined based on experience and calibrations.

In the case of Tangjiashan, a curve depicting the relationship between the discharge per unit width, Q/B, and the head, $H - z$, based on Eq. (4) with a value of 1.35 for C is drawn in Fig. 2 and compared with the measured values represented in Table 1.

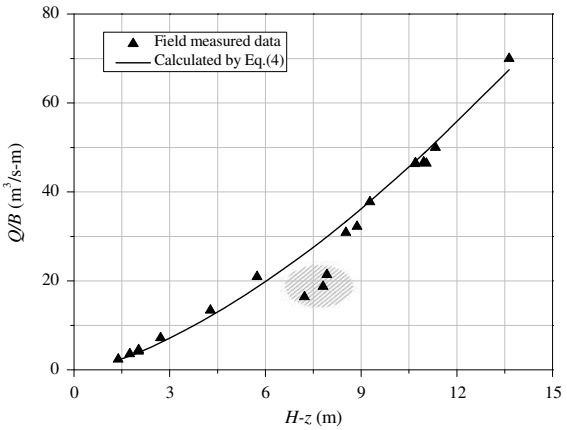

NOTE: (1) The solid line is calculated by Eq. (4) by taking m and C to be 0.8 and 1.35 respectively, (2) The dotted points are taken from Column 13 of Table 1. (3) The shaded zone represents the data taken between 6:30 to 8:30, June 10.

Fig. 2. Relationship between $(H - z)$ and Q/B

This shows a good agreement, except the data indicated with shading in Fig. 2, which are associated with the period between 6:30 a.m. and 8:30 a.m. on June 10. This value of C will be taken for the back analysis described later.

The flow velocity in the channel is determined by

$$V = \frac{C(H-z)^{3/2}}{h} \tag{5}$$

where h = flow depth. Fread (1988) and Singh et al. (1988) suggested using the following Manning equation to determine h:

$$h = \left(\frac{nQ}{BJ^{0.5}}\right)^{0.6} = \left[\frac{nC(H-z)^{1.5}}{J^{0.5}}\right]^{0.6} = \frac{n^{0.6}C^{0.6}(H-z)^{0.9}}{J^{0.3}} \tag{6}$$

The exponent of $(H-z)$ in Eq. (6), which is 0.9, is very close to unity. Therefore, the depth can be approximately estimated by a simplified relationship

$$h = m(H-z) \tag{7}$$

where m is defined as

$$m = \frac{h}{H-z} \approx \frac{n^{0.6}C^{0.6}}{J^{0.3}} \tag{8}$$

Eq. (8) shows that the value of m is related to the input of J, the slope of the channel. For example, associated with an input of $C = 1.36$ and $n = 0.025$, m changes from 1.04 to 0.26 as J changes from 0.001 to 0.1. As a matter of fact, the channel bed changes through the entire course of breach, whose slope cannot be determined with reasonable accuracy. On the other hand, the value of m has sound physical meaning, whose value can be virtually judged within a range, say $0.4 \sim 0.8$, if a landslide dam breach is concerned. As an alternative, the present study proposes an empirical method of using a trial value of m to determine h with Eq. (7). For the case of Tangjiashan, Column 12 in Table 1 shows that m ranges from 0.8 to 0.9. The back analysis in this paper calibrates m as 0.8. Sensitivity studies will be performed to review the effect of m on the calculated results.

Based on Eqs. (5) and (7), the flow velocity in the channel is

$$V = Cm^{-1}\sqrt{H-z} \tag{9}$$

The flow discharge Q given by Eq. (4) should be equal to the loss of reservoir water storage (Fread 1984; Singh et al. 1988), i.e.

$$Q = CB(H-z)^{3/2} = \frac{\Delta W}{\Delta H}\frac{\Delta H}{\Delta t} + q \tag{10}$$

where q = natural inflow into the reservoir; and W = reservoir water storage capacity, which is considered a function of water level H. To ensure that the increment of H is always positive in the calculations, ΔH is measured from time t to $t + \Delta t$, i.e.

$$\Delta H = H(t) - H(t + \Delta t) \tag{11}$$

Incipient Velocity and Shear Stress of Erosion

As discussed previously, the incipient velocity V_c at which soil erosion commenced for the Tangjiashan material was around 2.6 m/s, which was discussed by Liu et al. (2010) and found in general agreement with the criteria proposed by Neill (1968), García and Marza (1997), and the information summarized by Briaud (2008).

With regard to the incipient shear stress, Shields (1936) developed an empirical approach that involves the dimensionless shear stress as a function of the grain size and Reynolds number. His work was updated by Yalin and Karahan (1979) using carefully scrutinized, available experimental data, and subsequently improved further by Soulsby (1997). For other works on noncohesive material, refer to Egiazaroff (1965), van Rijn (1984), and Annandale (2006). These empirical models are used to calculate the incipient shear stress τ_c based on the relevant parameters of the Tangjiashan material, as summarized in Table 2. As discussed in the previous section, the incipient stress τ_c is believed to be within the range of 20–30 Pa (Column 14 in Table 1), which is calculated using Eq. (3).

The following empirical expressions proposed by various researchers have been used to calculate the incipient shear stresses, compared to the value of 20–30 Pa found in the case of Tangjiashan.

1. Schoklitsch (1914)

$$\tau_c = \sqrt{0.201\gamma(\gamma_s - \gamma)\lambda' d^3} \tag{12}$$

where λ' = shape factor, ($\lambda' = 1$, spherical particle; $\lambda' = 4$, flat particle); d = average particle size (m); γ_s = unit weight of sediment (N/m^3); γ = unit weight of water (N/m^3).

2. Shields (1936)

$$\frac{\tau_c}{(\gamma_s - \gamma)d} = fct(\mathrm{Re}_*) \tag{13}$$

where $fct(\mathrm{Re}_*)$ = 0.06 and 0.03, when $d \gg \delta$ and ($d \approx \delta$) respectively. d = average particle.

3. Egiazaroff (1965)

$$\frac{\tau_c}{(\gamma_s - \gamma)d} = \frac{0.1}{[\log 19(d/\bar{d})]^2} \tag{14}$$

where $\bar{d}$ = average diameter of grain for both gradation curves, for grains in movement, and for total sediments (m).

4. Van Rijn (1984)

$$\frac{\tau_c}{\rho(s-1)gd} = fct(d*) \tag{15}$$

where $fct(d^*) = 0.24\ d^{*-1}$, when $d^* \le 4 = 0.14\ d^{*-0.64}$, when $4 < d* \le 10 = 0.04$, when $10 < d* \le 20 = 0.013\ d^{*0.29}$, when

Table 2. Incipient Shear Stresses Determined by Criteria Proposed by Various Writers

Authors	Equation	Parameter adopted for Tangjiashan	Incipient shear stress (Pa)
Schoklitsch (1914)	Eq. (12)	$\gamma = 10{,}000$ N/m^3; $\gamma_s = 24{,}000$ N/m^3; $d = 0.005$ m; $\lambda' = 4$.	4.07
Shields (1936)	Eq. (13)	$\gamma = 10{,}000$ N/m^3; $\gamma_s = 24{,}000$ N/m^3; $d = 0.005$ m.	4.2
Egiazaroff (1965)	Eq. (14)	$\gamma = 10{,}000$ N/m^3; $d = 0.005$ m; $\gamma_s = 24{,}000$ N/m^3; $= 0.005$ m$\bar{d}$.	5.7
Van Rijn (1984)	Eq. (15)	$d = 0.005$ m;	11.32
Soulsby (1997)	Eq. (16)	$s = 2.65$; $\rho = 1{,}000$ kg/m^3; $v = 1.01 \times 10^{-6}$ m^2/s	11.26
Annandale (2006)	Eq. (17)	$\phi = 25°$; $\rho_s = 2{,}400$ kg/m^3; $d = 0.005$ m; $g = 9.8$ m^2/s; $\rho_w = 1{,}000$ kg/m^3.	23.2

$20 < d* \leq 150 = 0.056$, when $d* > 150$ respectively. $d* = d^* = d[(s-1)g/\nu^2]^{1/3}$ (m). d = average particle size.

5. Soulsby (1997)

$$\tau_c^* = \frac{0.30}{1+1.2d^*} + 0.055[1 - e^{(-0.02d^*)}] \tag{16}$$

where $d^* = d[(s-1)g/\nu^2]^{1/3}$ (m); d = average particle size (m); s = relative density; and ν = kinematic viscosity (m^2/s).

6. Annandale (2006)

$$\tau_c = \frac{2}{3} gd(\rho_s - \rho_w) \tan\phi \tag{17}$$

where ϕ = friction angle (°); ρ_s = mass density of soil (kg/m^3); and ρ_w = mass density of water (kg/m^3).

The calculated incipient shear stresses from these empirical models with the input associated with the case of Tangjiashan are summarized in Table 2 and found to be in general lower than the value of 20–30 Pa.

Soil Erosion Model

A large number of research works have dealt with the relationship between the soil erosion rate and shear stress for both cohesive and noncohesive materials. In general, an exponential expression has been proposed for noncohesive materials (Roberts et al. 1998; Gaucher et al. 2010)

$$\dot{z} = \frac{\Delta z}{\Delta t} = \Phi(\tau) = a_1(\tau - \tau_c)^{b_1} \tag{18}$$

where $\dot{z}$ = erosion rate in 10^{-3} mm/s; τ is in Pa; and time t is in seconds. a_1 and b_1 are coefficients either regressed from the test results or based on experience.

Similar to the definition for ΔH in Eq. (11), Δz is defined as an increment of z from t to $t + \Delta t$, i.e.

$$\Delta z = z(t) - z(t + \Delta t) \tag{19}$$

It has been found that most information regarding studies of Eq. (18) is based on small-scale laboratory tests rather than on the scale of Tangjiashan. For example, Gaucher et al. (2010) used a 5.5-m-long flume flow apparatus, which was only able to model sand material with an incipient velocity of up to 0.69 m/s. These experimental results could hardly be compared with the measured erosion rates in Tangjiashan.

Back analysis based on the measured erosion rates in Tangjiashan was performed with results of $a_1 = 8$ and $b_1 = 1.2$ in Eq. (18) and is shown in Fig. 3 by Curve A, given $\tau_c = 30$ Pa. Admittedly, this work is subjective, given the limited data and the large range of alternatives that could lead to different values of a_1 and b_1. In the sensitivity studies section, the impact caused by these variants will be studied further.

In this paper, a hyperbolic model is suggested, which takes the following form:

$$\dot{z} = \Phi(\tau) = \frac{v}{a + bv} \tag{20}$$

where v = shear stress with reference to its critical component

$$v = k(\tau - \tau_c) \tag{21}$$

and k = unit conversion factor that allows $\dot{z}$ to approach its asymptote $\dot{z}_{ult}$ within the working range of τ. Here, k is taken to be 100 with a unit of Pa for τ and 10^{-3} mm/s for $\dot{z}$. The hyperbolic curve has an asymptote represented by $\dot{z}_{ult} = 1/b$ as v approaches infinity, and $1/a$ represents the tangent of this curve at $v = 0$. This model is established based on the understanding that like a structural material, soil should not have unlimited strength against erosion. With reference to the measured data, a set of parameters $a = 1.1$, $b = 0.0007$, and $\tau_c = 30$ Pa is proposed, which results in curve B in Fig. 3 and gives $\dot{z}_{ult} = 1.429$ mm/s. This set of parameters will be used in the back analysis followed by sensitivity studies.

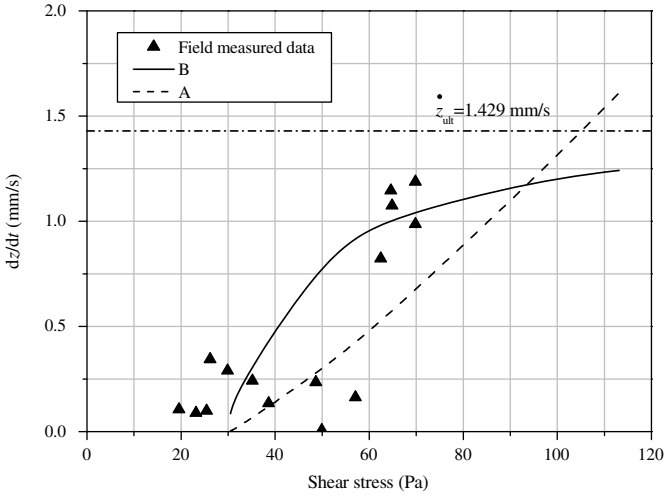

Fig. 3. Regressions on erosion rate parameters based on measured data: Line A is the exponential model represented by Eq. (12), $a_1 = 8$ and $b_1 = 1.2$; Line B is the hyperbolic model represented by Eq. (14), $a = 1.1$, $b = 0.0007$

Breach Lateral Enlargement Model

The lateral enlargement due to the collapse of the channel wall is the main mechanism of breach widening. In most of the existing breach models, this process is usually modeled using a wedge failure analysis with a straight line slip surface subjected to gravity and seepage forces (Fread 1988; Singh 1996; Wu 2013). However, the geotechnical profession has widely accepted more rigorous analytical methods with circular slip surfaces, such as Bishop's simplified method (1955) and the method proposed by the U.S. Army Corps of Engineers (1970). The procedure for calculating the factor of safety F is repeated among a variety of possible slip surfaces until a critical one associated with the minimum factor of safety F_m is found. This can be achieved by use of optimization methods (Chen and Shao 1988; Duncan 1996), then followed by a procedure to find the critical depth of toe-cutting that makes $F_m = 1$. The calculations can be performed by a computer program, for example, SLOPE/W (Krahn 2004) or STAB 2007 (Chen and Wang 2000).

In the lateral enlargement model, soil shear strength and internal friction angle are needed. Because the permeability of the landslide material could not allow free drainage during the rapid drawdown of the channel water surface and the pore water in the dam could hardly be determined by either analytical or empirical approaches with reasonable accuracy, the total stress analysis method, employing undrained shear strength parameters, is commonly used (Sherard et al. 1963; Lowe and Karafiath 1959; Johnson 1974). Two laboratory undrained triaxial tests have been conducted for the Tangjiashan saturated debris soil, denoted as samples A and B, with the gradations shown in Fig. 4, representing a coarse and a fine sample with $d_{50} = 17$ and 6 mm, respectively. They may be regarded as the upper and lower bounds of the grading

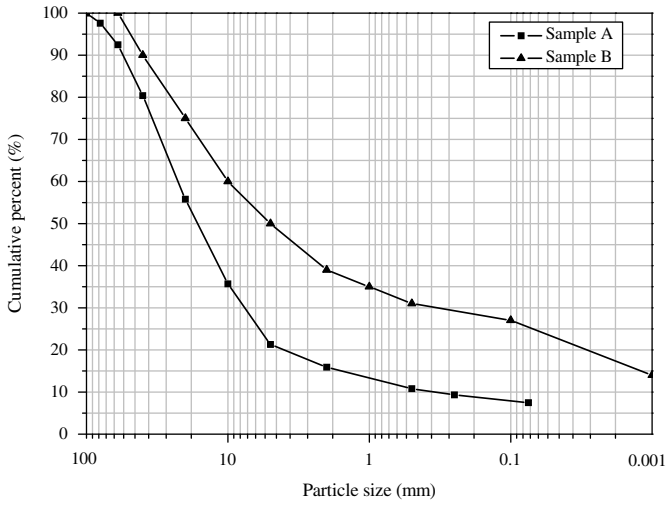

Fig. 4. Gradations of Tangjiashan material

curves given in Liu et al. (2010). The undrained triaxial test results are summarized in Table 3. In the back analysis, a set of total strength parameters $c_u = 25$ kPa and $\phi_u = 22°$ is adopted, followed by a sensitivity study that takes $c_u = 25$ kPa and $\phi_u = 26°$.

The lateral enlargement calculations for the Tangjiashan case are conducted in the following steps. Here, the initial excavated channel involves a slope inclined at 1.2 on 1 (horizontal to vertical) with a channel bed at an elevation of 740 m, and the soil shear strength parameters are $c_u = 25$ kPa and $\phi_u = 22°$.

Step 0: As shown in Fig. 5(a), an initially guessed circle obtained a factor of safety of 1.682. A critical slip surface can be found by STAB 2007 (Chen and Wang 2000) associated with $F_m = 1.437$ that is greater than 1. This means that the original slope is safe. It is worth noting that the critical slip surface calculated by STAB passes the toe of the slope exactly, which is common for this type of slope.

Step 1: With the erosion of the channel wall, the toe of the slope would be lower and move toward the bank. To simulate this erosion process, the toe of the slope in Step 0 was cut both vertically and horizontally by Δz, to create a new critical slope surface represented by ABCDEF in Fig. 5(a). By trial and error, it was found that a cut of $\Delta z = 3.2$ m would result in a critical slip surface with $F_m = 1.01$, as shown in Fig. 5(b). The geometry of this critical slip circle can be identified by its center coordinates (x_c, y_c) and radius R in combination with the toe elevation z_t. In this case, $x_c = 13.4$ m, $y_c = 778.3$ m, $R = 44.7$ m, and $z_t = 736.8$ m [Fig. 5(b)].

Step 2: This step adopted the residual part of the slope calculated in Step 1 with a slope surface ABCDEF in Fig. 5(b). Fig. 5(c) shows that the second landslide occurred associated with a value of $\Delta z = 1.3$ m as the toe was cut down to an elevation of 735.5 m.

The subsequent calculations followed the same procedure until the fifth step when the channel bed elevation reached 727 m, at which the right-hand side of the channel met the rock outcrops

Table 3. Undrained Triaxial Test Results

Item	Density	d_{50}	c_u	ϕ_u
Unit	g/cm^3	mm	kPa	°
Sample A	2.0	17	81.7	22
Sample B	1.9	6	20	18

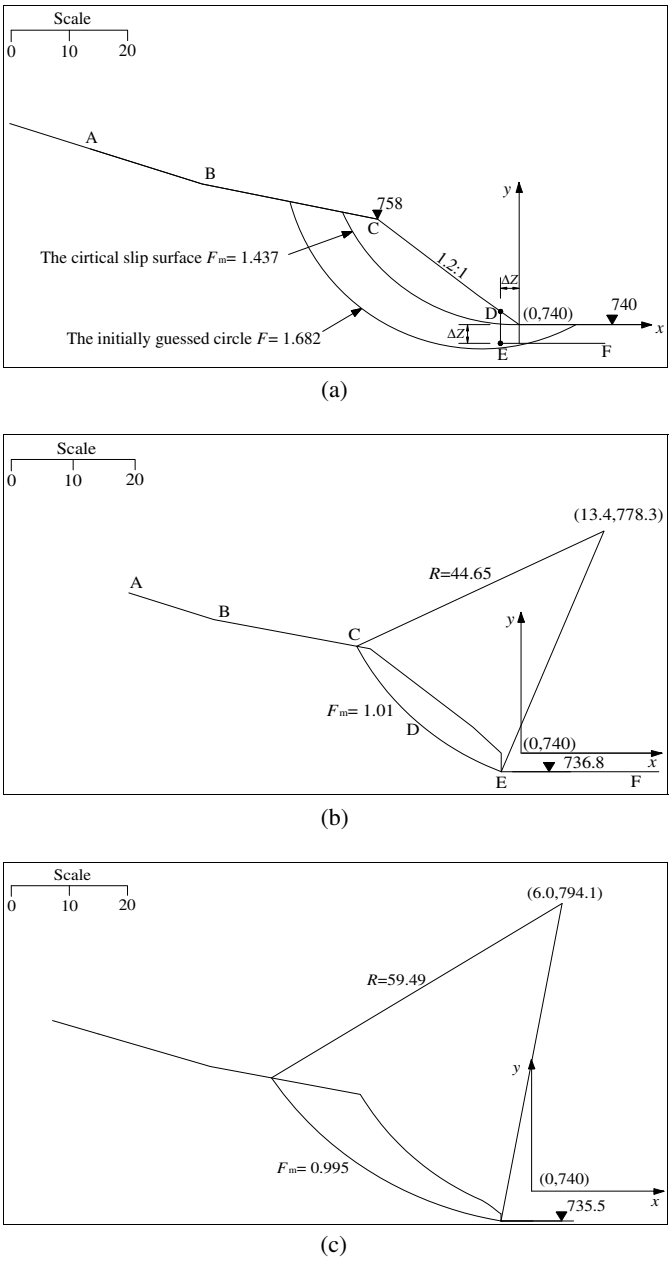

Fig. 5. Illustrations of landslide analysis of draining channel: (a) Step 0; (b) Step 1; (c) Step 2

(Liu et al. 2010). The predicted slip surfaces of the stepped landslide process are sketched in Fig. 6(a), and the details of the geometry are listed in Table 4.

In the numerical calculations, once the geometry of the channel is identified, the width of the channel water surface B can be calculated based on the water level at the channel H'. For example, it can be found in Table 1 that at 11:00 a.m., the channel bed elevation reached $z = 726.9$ m, the measured flow height was $h = 9.48$ m, and the measured water-surface width was $B = 129$ m. Based on the geometry described at the fifth step in Table 4, the calculated water-surface width B is $2 \times 66.18 = 132.36$ m, as illustrated in Fig. 6(b), which is quite close to the measured width.

The cross sections depicted in Fig. 6 are obviously more complex than the rectangular shape assumed in Eq. (4). As a conservative consideration, the calculated water-surface width is used as the average one of the cross section. Further improvement

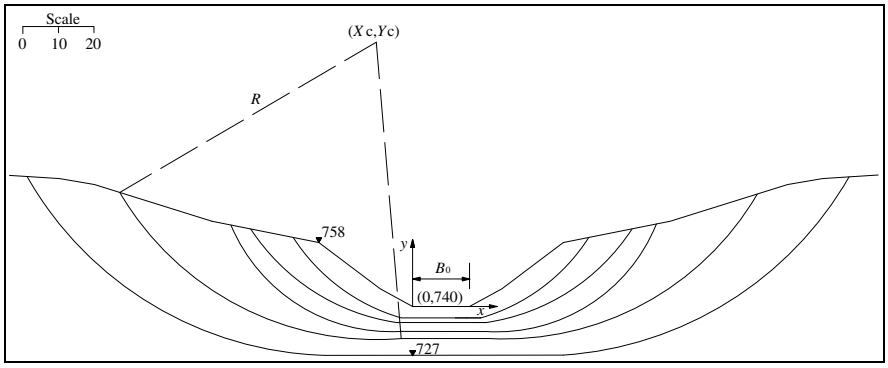

(a)

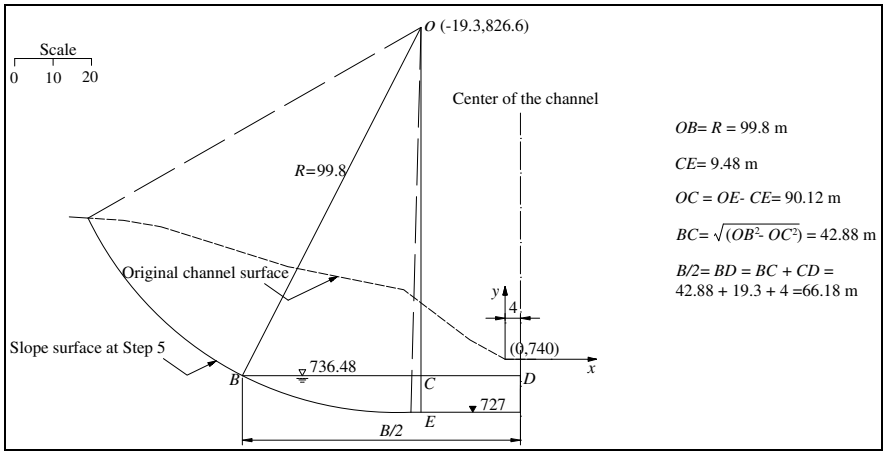

(b)

Fig. 6. Geometry of stepped landslides: (a) details of cross sections of stepped lateral enlargement, $c_u = 25$ kPa, $\phi_u = 22°$; (b) calculations of width of channel water surface at fifth lateral enlargement

Table 4. Geometry Information Identifying the Cross Section of Each Enlargement Step, $c_u = 25$ kPa, $\phi_u = 22°$

Step	X_c	Y_c	R	z_t
1	13.4	778.3	44.7	736.8
2	6.0	794.1	59.5	735.5
3	−4.3	788.6	55.6	733.0
4	−8.6	814.6	83.6	731.0
5	−19.3	826.6	99.8	727.0

may be considered by slightly adjusting the discharge coefficient C and putting a correction coefficient accounting for the geometry inconsistency involved.

Numerical Method

The breach analysis model described above requires solving Eqs. (10), either (18) or (19), and (9) for H, z, and V at a particular time step Δt. Numerical convergence can be a challenge because these equations are nonlinear and simultaneous. Conventional approaches (e.g., Fread 1988; Singh et al. 1988; Chang and Zhang 2010) start the calculation from an initial time t_0 with a given step Δt, for which the increments ΔH, Δz, and ΔV are obtained iteratively. By examining these equations, it can be found that once V is given, the solutions to ΔH, Δz, and Δt can be obtained by straightforward calculations without need of iteration. Therefore, a new approach is herein proposed that starts from an initial velocity V_0 with an interval of ΔV. The formulations and procedures of this new approach are described in the following subsections.

Formulations

At a velocity step from V_0 to $V_0 + \Delta V$, the average velocity V is

$$\bar{V} = V_0 + \Delta V/2 \tag{22}$$

The average values of H and z are

$$\bar{H} = H_0 - \Delta H/2 \tag{23}$$

$$\bar{z} = z_0 - \Delta z/2 \tag{24}$$

From Eq. (9), the average velocity can be found by

$$\bar{V} = Cm^{-1}\sqrt{(\bar{H} - \bar{z})} = Cm^{-1}\sqrt{\left(H_o - z_o + \frac{s}{2}\right)} \tag{25}$$

where

$$s = \Delta z - \Delta H \tag{26}$$

Once ΔV is given, $\bar{V}$ is obtained with Eq. (22), then s is obtained by reformulating Eq. (25) as

$$s = 2\left(\frac{m\bar{V}}{C}\right)^2 - 2(H_o - z_o) \tag{27}$$

Eqs. (10) and (18) or (20) can be expressed in finite difference forms, respectively, as

$$m\bar{V}B_o(H_o - z_o + 0.5s) - q = \frac{\Delta W}{\Delta H}\frac{\Delta H}{\Delta t} \tag{28}$$

$$\frac{\Delta z}{\Delta t} = \Phi(\bar{\tau}) \tag{29}$$

where $\bar{\tau}$ is determined by Eq. (3), in which V and h are replaced by their average values $\bar{V}$ and $\bar{h}$ determined by Eqs. (22) and (7), respectively.

Eliminating Δt and ΔH in Eqs. (28) and (29), one obtains

$$\Delta z = \frac{s}{1 - L} \tag{30}$$

where

$$L = \frac{A}{ED} \tag{31}$$

$$A = m\bar{V}B_o(H_o - z_o + 0.5s) - q \tag{32}$$

$$D = \Phi(\bar{\tau}) \tag{33}$$

$$E = \frac{\Delta W}{\Delta H} \tag{34}$$

Procedures

The calculation in a velocity step starts with a given ΔV based on the known values of H_0, z_0, and V_0 determined in the previous step. It includes the following computations

1. Calculate $\bar{V}$ by Eq. (22)
2. Calculate s by Eq. (27)
3. Calculate Δz by Eq. (30)
4. Calculate ΔH and Δt based on the known values of $\bar{V}$, s, and Δz from Eqs. (26) and (29), respectively.

The above procedures are straightforward. However, special treatments are required to make the calculation smoothly pass the point at which V attains its maximum V_m and ΔV transits from a positive to a negative value. The details are presented in the Appendix.

A spreadsheet entitled DB-IWHR 2014 is coded in Microsoft Excel 2007 with its VBA programming facilities. This program is simple, iteration-free, and transparent, allowing for quick prediction of the peak discharge of the breach flow. The spreadsheet and detailed information are available for download at the following website: http://www.geoeng.iwhr.com/geoeng/download.htm.

Back Analysis of the Breaching Process

The input parameters listed in Table 5 and adopted for the back analysis are based on the discussions in previous texts. In the numerical calculations, the breaching is assumed to start on June 10 at 6:00 a.m. The calculated results of the reservoir water level H, channel bed elevation z, water surface width B, flow discharge Q, and velocity V are plotted in Fig. 7, compared with the measured data taken from Table 1. For quantitative comparison, Table 6 gives various characteristic values obtained by field measurement and this back analysis, together with the results from subsequent sensitivity studies.

Table 5. Input Parameters for Back Analysis Case

Item	Parameters	Values	Notes
Natural inflow	q	80 m^3/s	
Initial breach width	B_o	16 m	Determined based on the draining channel geometry and a flow height of 3 m
Broad crested weir	C	1.35	Parameters involved in Eqs. (4) and (8)
	m	0.8	
Reservoir water storage	p_1	0.063	The relationship between the pool water level and storage for Eq. (10) can be found in Liu et al. (2010) and is approximated by $W = [p_1(H - H_r)^2 + p_2(H - H_r) + p_3] \times 10^6$ in m^3
	p_2	196.6	
	p_3	44	
	Hr	700 m	
Erosion rate	Vc	2.7 m/s	Parameters involved in Eq. (14)
	a	1.1	
	b	0.0007	
Lateral enlargement	—		Based on Table 4

The back analysis predicts a peak outflow of 7,610 m^3/s, compared with the measured value of 6,500 m^3/s. It can be found from Table 6 that all the calculated characteristic values agree with the measured data well before the peak outflow. After that moment, the calculated elevations of reservoir water and channel bed keep lowering while the field-measured data presented almost unchanged values. This may be explained by the sedimentation of a large amount of scoured material in the downstream river bed after the peak outflow. The coupled erosion and sedimentation effects should be considered if the model is expected to simulate the entire dam-breaching process. Another reason could be the heterogeneity of the landslide materials. The erosion stopped at the level of large rocks that had not been disintegrated and had much higher critical shear stress (Chang and Zhang 2010).

Sensitivity Studies

Determining the size and growth rate for breaches is not a precise exercise (Gee 2009). The concerted action on dam-break modelling (CADAM) Project report states that an estimate of ±50% for predicting peak discharge is suggested, with the accuracy of predicting the time of formation being considerably poor (Morris and Hassan 2002). Therefore, a sensitivity study should be a part of dam-breach analysis.

Sensitivity studies are conducted for the Tangjiashan dam breaching based on the back analysis case by changing one of the model parameters each time while keeping the others unchanged. The considered parameters and some of the model results are summarized in Table 6, with details being described below.

Case A: Parameters Related to the Broad-Crested Weir Flow

Cases A-1 and A-2 investigate the influence of taking different values of m, namely $m = 0.6$ and 0.5, respectively, compared with the value of $m = 0.8$ used in the back analysis case.

Case A-3 takes into account a higher value of C, which is 1.69, as proposed as an upper limit by Brater (1959) associated with $m = 0.5$. This case may present a presumably highest peak flow as far as the weir discharge coefficients are concerned.

From Fig. 8 and Table 6, it can be found that different hydraulic weir parameters have limited impact on the calculated peak

J. Hydraul. Eng., 2015, 141(4): 05014011

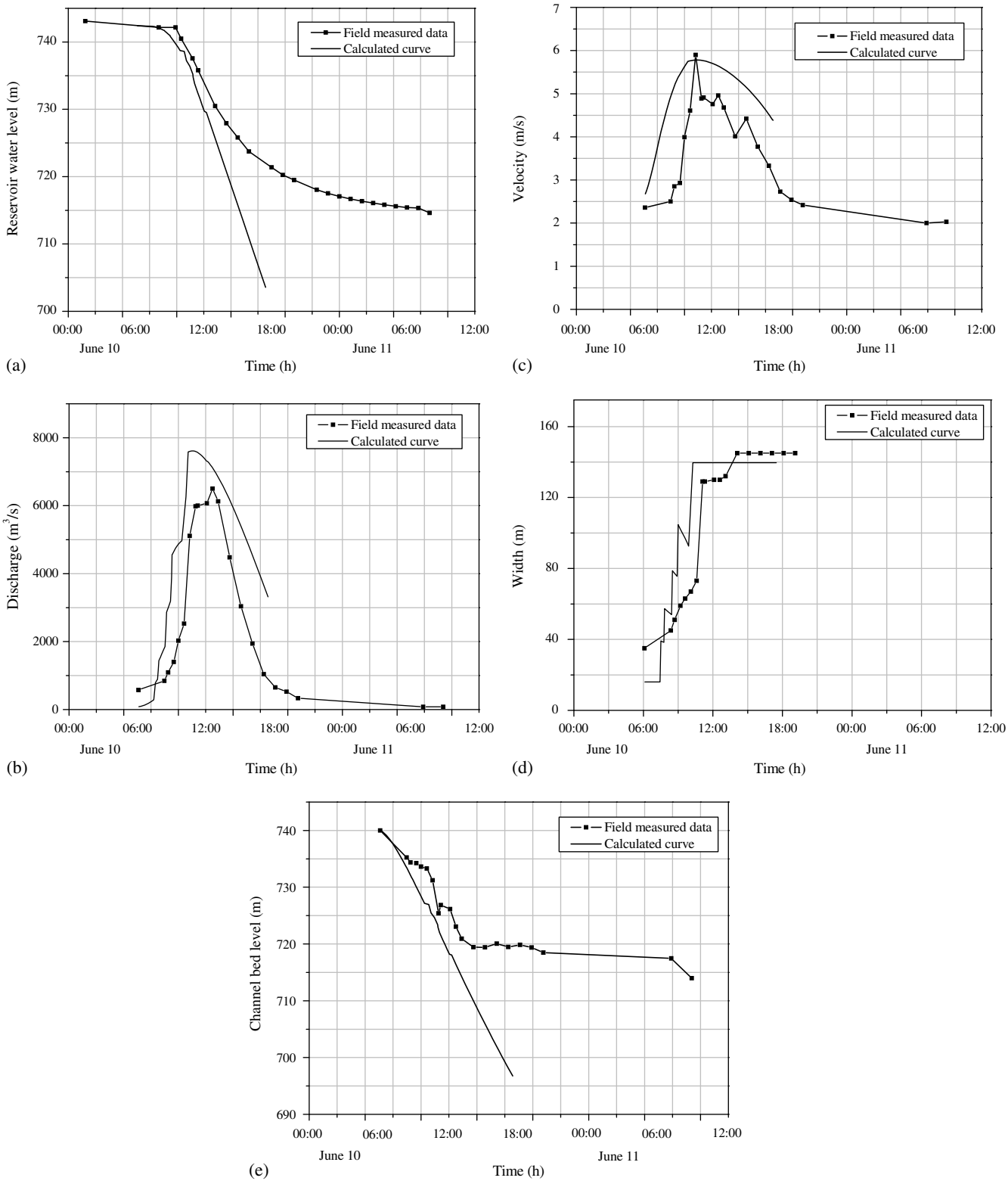

Fig. 7. Calculated results versus time compared with measured data: (a) reservoir water level; (b) flow discharge; (c) velocity; (d) flow surface width; (e) channel bed level

discharges. Case A-3, which is presumed to be an upper bound of the peak outflow, is 8,300 m^3/s, compared to 7,610 m^3/s of the back analysis case. From a practical point of view, one may assume a lower value of m, and a higher one for C, based on experience as a conservative approach to find the maximum possible peak outflow.

Case B: Parameters Related to Hyperbolic Erosion Model

Comparing with the back analysis case that takes $a = 1.1$ and $b = 0.0007$ in the hyperbolic model expressed by Eq. (20), Case B-1 takes $a = 1.0$ and $b = 0.0005$, while Case B-2 has $a = 0.9$ and

Table 6. Summaries of Characteristic Parameters for Sensitivity Studies

				Peak flow				Peak velocity	
				t_m	H	z	Q_m	V_m	dz/dt
Number	Case	Values	Equation number	Hour	m	m	m^3/s	m/s	mm/s
Field measurement				12:30	732.25	720.9	6,500	4.96	1.19
Back analysis case				11:02	735.21	723.41	7,609.97	5.78	1.16
A	A − 1	$m = 0.6$, $C = 1.35$	Eqs. (4) and (8)	11:12	730.04	717.36	7,829.65	7.60	1.31
	A − 2	$m = 0.5$, $C = 1.35$	Eq. (8)	11:16	729.49	716.40	7,858.80	6.54	1.35
	A − 3	$m = 0.5$, $C = 1.69$	Eq. (8)	10:27	731.31	719.52	8,300.19	5.89	1.38
B	B − 1	$a = 1.0$, $b = 0.0005$	Eq. (14)	10:57	730.55	717.06	9,475.62	6.18	1.58
	B − 2	$a = 0.9$, $b = 0.0003$	Eq. (14)	10:26	724.61	707.10	13,524.99	7.05	2.54
C	C − 1	$a_1 = 8$, $b_1 = 1.2$	Eq. (12)	16:53	730.04	718.25	7,512.91	5.78	1.24
	C − 2	$a_1 = 10$, $b_1 = 1.2$	Eq. (12)	15:31	724.96	710.53	10,357.93	6.39	1.94
	C − 3	$a_1 = 8$, $b_1 = 1.3$	Eq. (12)	15:11	718.77	699.59	15,192.20	7.37	3.35
D	D − 1	Table 4		13:26	727.36	712.54	6,740.95	6.48	1.20

Note: dz/dt = erosion rate; H = water level; Q_m = discharge; t_m = occurring time; V_m = peak velocity; z = channel bed level.

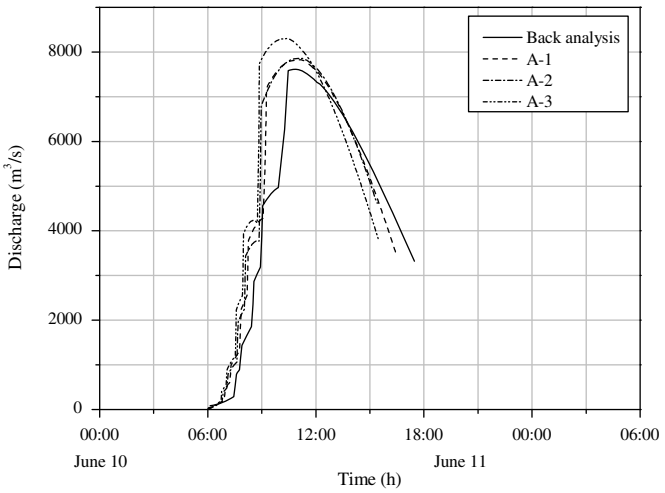

Fig. 8. Sensitivity studies of Case A: curves of flow discharges versus time

$b = 0.0003$. They represent two more sets of erodible soils. The hydrograph of Case B-2 adopts an ultimate erosion rate of $\dot{z}_{ult} = 1/b = 3.3$ mm/s, which is three times that of the maximum measured rate shown in column 15 of Table 1 (= 1.19 mm/s). Referring to Table 6 and Fig. 9, the peak discharge of Case B-2 is 13,000 m^3/s, which is nearly double the values of the field measurement and the back analysis case. This indicates that the hyperbolic model could handle a large range of possible parameter inputs.

Conceptually speaking, the field measurement of 1.19 mm/s could be presumed as a close estimate to $\dot{z}_{ult} = 1/b$, which is the maximum possible erosion rate for the material in Tangjiashan because the reservoir still had sufficient energy at that time to increase this if the soil could have resisted it. The maximum possible erosion rate $\dot{z}_{ult}$ has physical meaning, and the use of the hyperbolic model could help experienced engineers reduce the risk caused by the use of inappropriate erosion parameters.

Case C: Parameters Related to Exponential Erosion Model

Case C-1 investigates the exponential erosion model of Eq. (18) with the parameters $a_1 = 8$ and $b_1 = 1.2$, as denoted by Curve

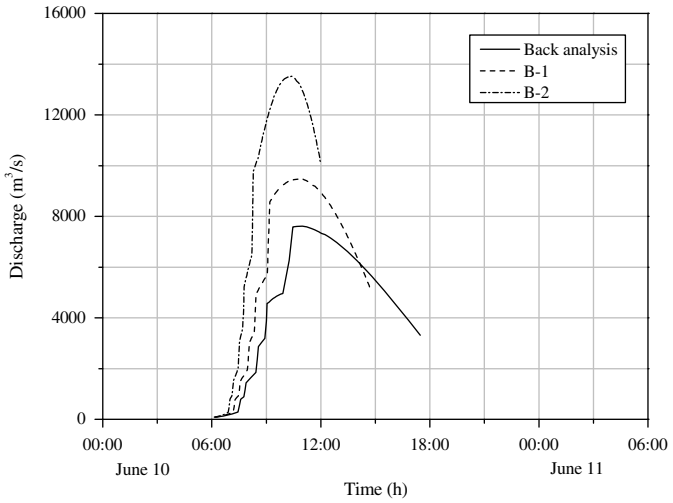

Fig. 9. Sensitivity studies of Case B: curves of flow discharges versus time

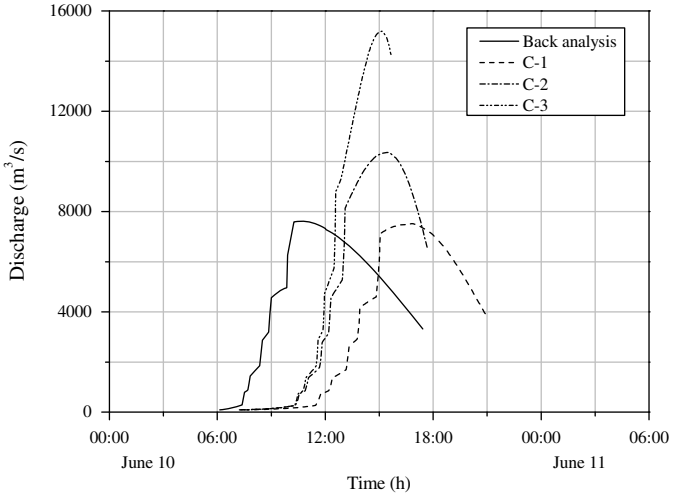

Fig. 10. Sensitivity studies of Case C: curves of flow discharges versus time

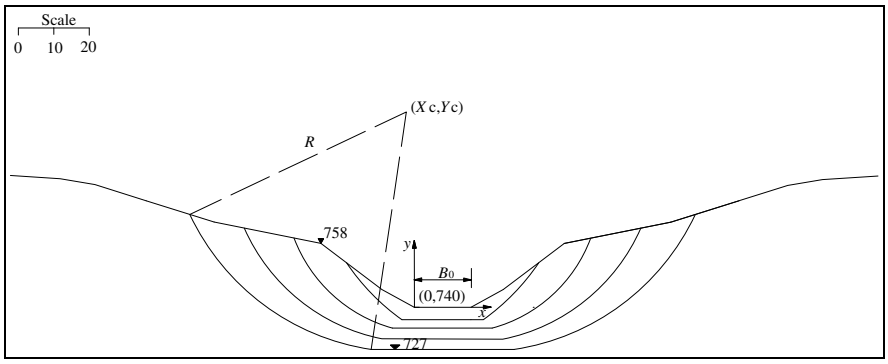

Fig. 11. Details of the cross sections of stepped lateral enlargement, $c_u = 25$ kPa, $\phi_u = 26°$

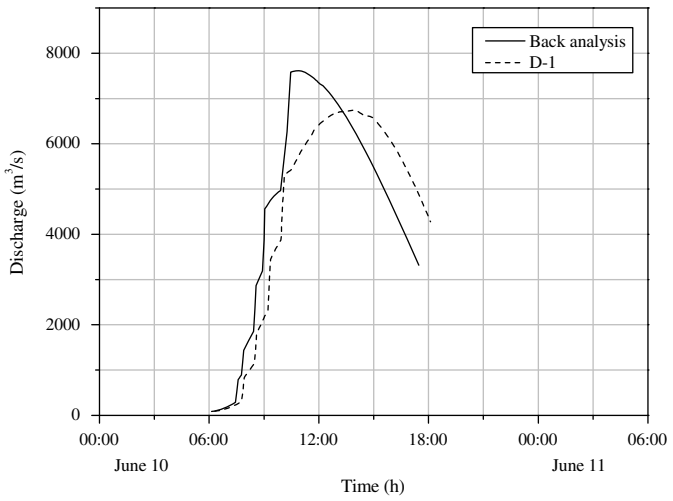

Fig. 12. Sensitivity studies of Case D: curves of flow discharges versus time

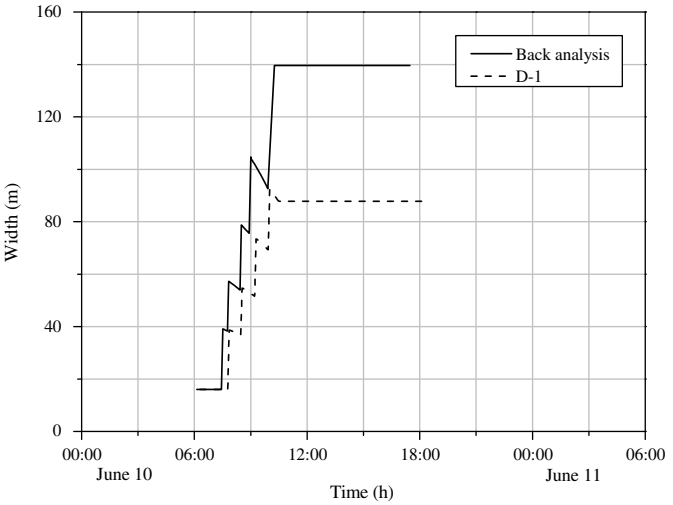

Fig. 13. Sensitivity studies of Case D: curves of water surface width versus time

A in Fig. 3, and a prediction of Q_m of 7,512.9 m^3/s, as listed in Table 6. Case C-1 takes more time to reach peak outflow compared with other cases adopting the hyperbolic model. This might still be acceptable because the time at which the channel erosion started cannot be identified exactly from Table 1.

Similar to the investigations on the hyperbolic model, two more sets of values for erosion parameters, namely, $a_1 = 10$ and $b_1 = 1.2$ and $a_1 = 8$ and $b_1 = 1.3$ have been assigned as Cases C-2 and C-3, respectively. The peak discharges shown in Fig. 10 exhibit large differences. Compared with the peak discharges obtained with field measurements and in the back analysis case, Case C-3 shows that a slight change of b_1 from 1.2 to 1.3 would double the peak outflow. Thus, the use of the exponential erosion model encounters the difficulties of assigning proper parameters for soil erosion.

Case D: Parameters Related to Lateral Enlargement

Studies on the uncertainties involved in the channel lateral enlargement analysis are focused on the variance of shear strength parameters. Case D-1 investigates a set of higher values of strength parameters: $c_u = 25$ kPa and $\phi_u = 26°$. Following the procedures for calculating the stepped landslides described in the subsection breach lateral enlargement model, the computation ended at the fourth step, resulting in an enlarged cross section, as shown in Fig. 11, which is smaller in size compared with the back analysis case shown in Fig. 6. The calculated peak flow discharge in this case is 6,740 m^3/s, as shown in Table 6 and Fig. 12, compared with 7,610 m^3/s of the back analysis case. Fig. 13 shows that the water-surface width at the channel bed elevation of 726 m is only 90 m, which is much smaller than the 140 m in the back analysis case shown in Fig. 7(d). However, the peak outflow does not reduce considerably.

Concluding Remarks

The draining process of the Tangjiashan barrier lake is investigated as a prototype test against the existing theoretical framework and related parameters of dam breach model. The main findings are:

1. The dam breach analysis model proposed in this paper is capable of reproducing the dam-break hydrograph measured for the Tangjiashan barrier lake, if the input values of the various parameters are selected carefully, based on the field information. As far as the Tangjiashan landslide debris material is concerned, the key feature is that the erosion rate should lie between 0.4 and 1.1 mm/s, which is associated with a flow velocity range of 3–6 m/s and a shear stress range of 20–100 Pa.
2. The sensitivity studies indicate that among all of the parameters affecting the calculated results, the soil erosion

rate is of critical importance. The present study suggests a hyperbolic model that is used with an asymptote of the ultimate erosion rate. This model is based on the understanding that analogous to a structural material, soil should have a strength beyond which the erosion rate would yield. With this hyperbolic model, the dam-breach model is reasonably less sensitive to the input of erosion parameters.

3. This paper adopts a new solution technique that integrates the flow process in terms of velocity increment and solves the governing equations directly without iteration. This straightforward solution method has been coded in an Excel spreadsheet, providing easy, transparent access to practitioners working on dam-breach analysis.

Appendix. Numerical Treatments at the Point Where the Flow Velocity Approaches Its Maximum

At the point that V is equal to its maximum V_m, $dV/dt = 0$. From Eq. (18) or (20), the erosion rate is always greater than zero, i.e., $\Delta z/\Delta t > 0$. It can then be concluded that (Fig. 14)

$$\begin{aligned} &\text{As } V < V_m, \quad \frac{dV}{dt} > 0, \quad \frac{dV}{dz} = \frac{dV}{dt}\frac{dt}{dz} > 0 \\ &\text{As } V = V_m, \quad \frac{dV}{dt} = 0, \quad \frac{dV}{dz} = \frac{dV}{dt}\frac{dt}{dz} = 0 \\ &\text{As } V > V_m, \quad \frac{dV}{dt} < 0, \quad \frac{dV}{dz} = \frac{dV}{dt}\frac{dt}{dz} < 0 \end{aligned} \tag{35}$$

With the above understanding, it has been found that when V is approaching its maximum, the calculation of Δz by Eq. (30) involves a division between two very small values. This statement is demonstrated as follows:

As $dV/dt = 0$, from Eq. (9), we have

$$\frac{d(H-z)}{dt} = 0 \tag{36}$$

Therefore,

$$\Delta H = \Delta z \tag{37}$$

With the definition for s by Eq. (26), we have

$$s = 0 \tag{38}$$

By substituting Eqs. (37) and (38) into Eqs. (28) and (29) and eliminating Δt, we have

$$L - 1 = \frac{A}{ED} - 1 = 0 \tag{39}$$

Conditions Eqs. (38) and (39) mean that as V approaches its maximum, calculations would occasionally result in an abnormal value of Δz calculated by Eq. (30); it would be either extremely large or negative, due to the limited computational precision. To allow the integration process to pass the peak value of V_m smoothly, the following treatments have been adopted.

First, the input of ΔV would be decreased automatically as the value of $(L - 1)$ approaches zero. In this program, it was set that ΔV would be reduced gradually to 0.005 m/s when L is greater than 0.9. In the meantime, both a positive and a negative ΔV would be tried in the subsequent calculations, and the following three cases would be encountered with corresponding treatments.

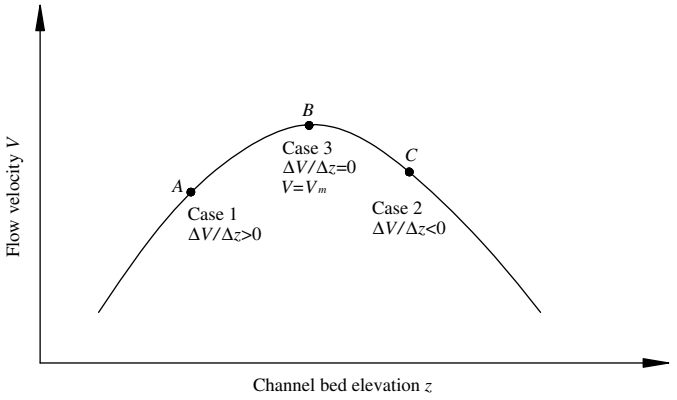

Fig. 14. Treatments as flow velocity approaches its maximum

Case 1: The values of positive and negative ΔV result in positive and negative values of Δz from Eq. (30), respectively, as represented by Point A in Fig. 14. This means that the integration is still following its normal process with an increasing ΔV implemented at the left side of the peak. The next step takes a procedure similar to the previous one with both positive and negative ΔV.

Case 2: The positive and negative values of ΔV result in negative and positive values of Δz, respectively, as represented by Point C in Fig. 14. Based on Eq. (35), it can be found that the integration is actually implemented right at the range of the peak. The transition of the curve through the peak has been successfully realized in the previous integration step. The solution associated with the negative value of ΔV should be the true answer, and it should be adopted. The next step of the computation proceeds with a negative value of ΔV only.

Case 3: The numerical algorithm occasionally falls into a trap, as represented by Point B in Fig. 14, where the use of Eq. (30) results in an abnormal value of Δz because the values of both s and $(1 - L)$ are very small. Experience has shown that this situation would most likely occur when

$$0.985 < L < 1.015 \tag{40}$$

At this point, where V attains its maximum, we have

$$V_o = V_m - \frac{dV}{dz}\Delta z - \frac{1}{2}\frac{d^2V}{dz^2}\Delta z^2 = V_m - \frac{1}{2}\frac{d^2V}{dz^2}\Delta z^2 \tag{41}$$

where V_o = initial velocity of this step. Instead of Eq. (30), the following equation can be used to find Δz

$$\Delta z = \sqrt{-\frac{2(V_o - V_m)}{d^2V/dz^2}} = \sqrt{\frac{2\Delta V}{d^2V/dz^2}} \tag{42}$$

The value of d^2V/dz^2 can be calculated based on the information obtained in the previous two steps.

Table 7 shows the calculation details for the back analysis case that encountered Case 3. When the calculation proceeded to $H = 736.345$ m, as represented by Row 3, an increment of 0.005 m/s for V gave an L of 1.008 (Column 6), which is very close to unity. As a result, the value of Δz calculated by Eq. (30), and indicated in Column 7, is a negative value of -2.949 m. In Columns 8 to 10 a negative increment of 0.005 m/s was tried for V, which also gave a negative value

Table 7. Calculation Details for Back Analysis Case That Encountered Case 3

					$V+\Delta V$			$V-\Delta V$				
Step number	H	z	V	ΔV	s	L	Δz	s	L	Δz	d^2V/dz^2	Δz (final)
1	738.599	727.013	5.730	0.02	0.083	0.625	0.221	−0.079	0.609	−0.201	−0.004	0.221
2	738.460	726.792	5.751	0.02	0.083	0.962	2.199	−0.079	0.773	−0.349	−0.067	2.199
3	736.345	724.594	5.771	0.005	0.022	1.008	−2.949	−0.018	0.984	−1.129	0.003	0.386
4	735.982	724.208	5.777	−0.005	−0.018	1.015	1.216	0.022	0.995	4.790	−0.021	1.216
5	734.747	722.992	5.772	−0.005	−0.018	1.038	0.484	0.022	1.018	−1.267	−0.007	0.484

of −1.129 m. This problem comes from insufficient computational precision, which can be solved by using Eq. (42). A value of 0.386 m was obtained at Column 12 for Δz. The next step adopted a negative velocity increment, as shown in Row 4, and the calculation successfully passed the transit point of V_m.

Acknowledgments

This research work was supported by National Basic Research Program of China (Grant No. 2013CB0364) and National Natural Science Foundation of China (Grant No. 51109001 and 51309260). The authors are indebted to the associate editor who made significant discussions and great efforts in editing the manuscript.

References

Annandale, G. W. (2006). *Scour technology*, McGraw-Hill, New York, 430.
ASCE/EWRI (Environmental and Water Resources Institute) Task Committee on Dam/Levee Breaching. (2011). "Earthen embankment breaching." *J. Hydraul. Eng.*, 1549–1564.
Bishop, A. W. (1955). "The use of the slip circle in the stability analysis of slopes." *J. Geotech.*, 5(1), 7–17.
Brater, E. (1959). "Hydraulics." *Civil engineering handbook*, L. C. Urquhart, ed., McGraw-Hill Book, New York, 4.44–4.60.
Briaud, J. L. (2008). "Case histories in soil and rock erosion: Woodrow Wilson Bridge, Brazos River, Meander, Normandy Cliffs, and New Orleans Levees." *J. Geotech. Geoenviron. Eng.*, 1425–1447.
Brown, R. J., and Rogers, D. C. (1977). "A simulation of the hydraulic events during and following the Teton Dam failure." *Proc., Dam-Break Flood Routing Workshop*, Washington, DC, 131–163.
Brown, R. J., and Rogers, D. C. (1981). *BRDAM users manual*, U.S. Dept. of the Interior, Water and Power Resources Service, Denver, 67.
Chang, D. S., and Zhang, L. M. (2010). "Simulation of the erosion process of landslide dams due to overtopping considering variations in soil erodibility along depth." *Nat. Hazards Earth Syst. Sci.*, 10(4), 933–946.
Chen, Z. Y., and Shao, C. M. (1988). "Evaluation of minimum factor of safety in slope stability analysis." *Can. Geotech. J.*, 25(4), 735–748.
Chen, Z. Y., and Wang, X. G. (2000). "Chaper12: Rock slope engineering." *Large dams in China*, J. Z. Pan and J. He, eds., China Hydropower Press, Beijing, 695–721.
Costa, J. E. (1985). "Floods from dam failures." *U.S. Geological Survey Open-File Rep. No. 85-560*, U.S. Geological Survey, Denver.
Cristofano, E. A. (1965). *Method of computing erosion rate of failure of earth dams*, U.S. Bureau of Reclamation, Denver.
Duncan, J. (1996). "State of the art: Limit equilibrium and finite-element analysis of slopes." *J. Geotech. Eng.*, 10.1061/(ASCE)0733-9410(1996)122:7(577), 577–596.
Egiazaroff, I. V. (1965). "Calculation of nonuniform sediment concentrations." *J. Hydraul. Div.*, 91(4), 225–247.
Fread, D. L. (1984). *DAMBRK: The NWS dam break flood forecasting model*, National Oceanic and Atmospheric Administration, National Weather Service, Silver Spring, MD.
Fread, D. L. (1988). *BREACH: An erosion model for earthen dam failures (model description and user manual)*, National Oceanic and Atmospheric Administration, National Weather Service, Silver Spring, MD.
Froehlich, D. C. (1995). "Peak outflow from breached embankment dam." *J. Water Resour. Plann. Manage.*, 10.1061/(ASCE)0733-9496(1995)121:1(90), 90–97.
García, M. H., and Marza, J. A. (1997). "Sedimentation and protection." Chapter 8, *Manual of engineering rivers*, Series 592, delInstituto de Ingeniería, UNAM, Mexico (in Spanish).
Gaucher, J., Marche, C., and Mahdi, T. F. (2010). "Experimental investigation of the hydraulic erosion of noncohesive compacted soils." *J. Hydraul. Eng.*, 901–913.
Gee, D. (2009). "Comparison of dam breach parameter estimators." *World Environmental and Water Resources Congress 2009*, U.S. Army Corps of Engineers, Hydrologic Engineering Center, Davis, CA, 1–10.
Guo, Q. C., and Jin, Y. C. (1999). "Modeling sediment transport using depth-averaged and moment equations." *J. Hydraul. Eng.*, 1262–1269.
Harris, G. W., and Wagner, D. A. (1967). "Outflow from breached earth dams." B.Sc. thesis, Dept. of Civil Engineering, Univ. of Utah, Salt Lake City.
Hassan, M., and Morris, M. W. (2008). "IMPACT project field tests data analysis." *FLOOD site, Rep. No. T04-08-04*, European Community's Sixth Framework Programme, U.K.
Hydrologic Engineering Center (HEC). (2006a). "HEC-HMS user's manual." *Version 3.1.0, CPD-74A*, U.S. Army Corps of Engineers, Hydrologic Engineering Center, Davis, CA.
Hydrologic Engineering Center (HEC). (2006b). "HEC-RAS User's Manual." *Version 4.0 beta, CPD-68*, U.S. Army Corps of Engineers, Hydrologic Engineering Center, Davis, CA.
Jack, R. (1996). "The mechanics of embankment failure due to overtopping flow." Master's thesis, Univ. of Auckland, Auckland, New Zealand.
Johnson, J. J. (1974). "Analysis and design relating to embankments." *Proc., Conf. on Analysis and design in Geotechnical Engineering*, ASCE, New York, Vol. 2, 1–48.
Krahn, J. (2004). "Stability modeling with Slope/W." *An engineering methodology*, Geo-Slope/W International, Calgary, AB, Canada.
Liu, N., Chen, Z., Zhang, J., Lin, W., Chen, W., and Xu, W. (2010). "Draining the Tangjiashan barrier lake." *J. Hydraul. Eng.*, 914–923.
Liu, N., Zhang, J. X., Lin, W., Cheng, W. Y., and Chen, Z. Y. (2009). "Draining Tangjiashan Barrier Lake after Wenchuan earthquake and the flood propagation after the dam break." *Sci. China Ser. E: Technol. Sci.*, 52(4), 801–809.
Lowe, J., III, and Karafiath, L. (1959). "Stability of earth dam upon drawdown." *First Pan-American Conf. on Soil Mechanics and Foundation Engineering*, Mexico City.
Macchione, F. (2008). "Model for predicting floods due to earthen dam breaching. I: Formulation and evaluation." *J. Hydraul. Eng.*, 10.1061/(ASCE)0733-9429(2008)134:12(1688), 1688–1696.
MacDonald, T. C., and Langridge-Monopolis, J. (1984). "Breaching characteristics of dam failures." *J. Hydraul. Eng.*, 10.1061/(ASCE)0733-9429(1984)110:5(567), 567–586.
Morris, M. W., and Hassan, M. A. (2002). "Breach formation through embankment dams and flood defence embankments: A state of the art review." *HR Wallingford, IMPACT-Project Workshop Paper*, Wallingford, U.K.
Neill, C. R. (1968). "Note on initial movement of coarse uniform bed-material." *J. Hydraul. Res.*, 6(2), 173–176.
Peng, M., and Zhang, L. M. (2012). "Breaching parameters of landslide dams." *Landslides*, 9(1), 13–31.

Ponce, V. M., and Tsivoglou, A. J. (1981). "Modeling gradual dam breaches." *J. Hydraul. Div. (Proc. Am. Soc. Civil Eng.)*, 107(HY7), 829–838.
Roberts, J., Jepsen, R., Gotthard, D., and Lick, W. (1998). "Effects of particle size and bulk density on erosion of quartz particles." *J. Hydraul Eng.*, 1261–1267.
Schoklistch, A. (1914). *On the drag force of sediment movement*, Engelmann, Leipzige, Germany (in German).
Sherard, J., Woodward, R., Gzienski, S., and Clevenger, W. (1963). "Failures and damages." *Earth and earth-rock dams*, 1st Ed., Wiley, New York, 130–131.
Shields, A. (1936). "Application of similarity principles and turbulence research to bed-load movement." *Rep. No. 167*, California Institute of Technology, Pasadena, CA.
Singh, V. P. (1996). *Dam breaching modeling technology*, Kluwer Academic Publishers, Dordrecht, Netherlands.
Singh, V. P., and Scarlatos, P. D. (1988). "Analysis of gradual earth-dam failure." *J. Hydraul. Eng.*, 21–42.
Singh, V. P., Scarlatos, P. D., Collins, J. G., and Jourdan, M. R. (1988). "Breach erosion of earth-fill dams (BEED) model." *Nat. Hazard.*, 1(2), 161–180.
Soulsby, R. L. (1997). *Dynamics of marine sands*, Thomas Telford, London.
U.S. Army Corps of Engineers. (1970). "Engineering and design, stability of earth and rock-fill dams." *Engineer manual*, Dept. of the Army, Corps of Engineers, Washington, DC.
Van Rijn, L. C. (1984). "Sediment transport. Part I: Bed load transport." *J. Hydraul. Eng.*, 1431–1456.
Wahl, T. L. (2004). "Uncertainty of predictions of embankment dam breach parameters." *J. Hydraul. Eng.*, 389–397.
Wahl, T. L. (2010). "Dam breach modeling—An overview of analysis methods." *Joint Federal Interagency Conf. on Sedimentation and Hydrologic Modeling*, Las Vegas.
Walder, J. S., and O'Connor, J. E. (1997). "Methods for predicting peak discharge of floods caused by failure of natural and constructed earth dams." *Water Resour. Res.*, 33(10), 12.
Wang, Z., and Bowles, D. S. (2006). "Three-dimensional noncohesive earthen dam breach model. Part I: Theory and methodology." *Adv. Water Resour.*, 29(10), 1528–1545.
Wu, W. (2013). "Simplified physically based model of earthen embankment breaching." *J. Hydraul. Eng.*, 837–851.
Wu, W., and Wang, S. S. (2010). "An introduction to latest developments in soil erosion and sediment transport modeling." *11th Int. Symp. on River Sedimentation, Sedimentation and Sustainable Use of River System*, Sun Media (Pty), Toronto, Canada.
Wurbs, R. A. (1987). "Dam-breach flood wave models." *J. Hydraul. Eng.*, 29–46.
Yalin, M. S., and Karahan, E. (1979). "Inception of sediment transport." *J. Hydraul. Div. Am. Soc. Civ.*, 105(11), 1433–1443.
Zhang, J., Li, Y., Xuan, G., Wang, X., and Li, J. (2009). "Overtopping breaching of cohesive homogeneous earth dam with different cohesive strength." *Sci. China Ser. E: Technol. Sci.*, 52(10), 3024–3029.
Zhu, Y. H., Visser, P. J., and Vrijling, J. K. (2004). "Review on embankment dam breach modeling." *New developments in dam engineering*, Taylor & Francis Group, London, 1189–1196.